A&A 377, 264–272 (2001)
DOI: 10.1051/0004-6361:20011002

Astronomy & Astrophysics

Doppler imaging of stellar surface structure

XVII. The solar-type Pleiades star HII 314 = V1038 Tauri

J. B. Rice[1,⋆] and K. G. Strassmeier[2,⋆]

[1] Department of Physics, Brandon University, Brandon, Manitoba R7A 6A9, Canada
e-mail: rice@BrandonU.ca
[2] Astrophysical Institute Potsdam, An der Sternwarte 16, 14482 Potsdam, Germany

Received 29 May 2001 / Accepted 10 July 2001

Abstract. We present the first Doppler image of a solar-type G dwarf in the Pleiades open cluster. As such, the star represents the Sun at an age of approximately 100 Myr and could be an important target for further progress in magnetic-braking and angular-momentum-transport theories. Our image reconstructions were done from a full spectrum inversion with a total of 38 spectral lines but we also present single-line inversions using the prominent Li I 6707-Å line and the nearby Ca I 6717-Å line. The maps reveal cool spots at or near the pole and within the equatorial regions, in contradiction to our predictions from flux-tube modelling that only medium-latitude spots should be seen. The maps also show several warm spots near the equatorial regions but their reality needs to be confirmed. A polar spot is recovered but likely consists of several smaller spots at very high latitudes touching the visible pole instead of a big cap-like spot as seen on some RS CVn binaries.

Key words. stars: activity – starspots – stars: imaging – stars: individual: HII 314 – stars: late-type

1. Surface imaging of solar-type stars in open clusters

Magnetic braking of stellar rotation due to a stellar wind along predominantly equatorial magnetic field lines, as worked for our Sun, seems unable in every case to be effective in slowing down stars from their initial angular momentum gained during the contraction of the pre-stellar cloud. The ultra-fast rotators (UFRs) in the young open clusters α Per (age ≈50 Myr) and Pleiades (age ≈100 Myr) as well as the young field stars AB Dor, LQ Hya, EK Dra are the most cited examples. Their simple existence is something of a problem since magnetic braking of a solar-mass star should have had, by the age of these stars, enough time during pre-main-sequence evolution to halt the rapid rotation. Accretion disks in the early pre-main sequence stages certainly play an important and maybe dominant role in explaining the angular momentum loss of very young objects but cannot easily be incorporated into an explanation of the existence of several hundreds of cluster-ZAMS stars that are not in a close binary but still rapidly rotating (Stauffer et al. 1984; Soderblom et al. 1993b; O'Dell et al. 1995; Barnes & Sofia 1996; and others).

What process then might allow these stars to maintain their angular momentum? The currently favored hypothesis is the onset of a dynamo saturation, i.e. a saturation of the atmospheric (coronal) volume with magnetic fields (Vilhu 1984; Keppens et al. 1995) so that there is no torque arm for magnetic braking via a stellar wind. For further reading we refer to Mestel (1999).

Solanki et al. (1997) and Buzasi (1997) – and later Strassmeier et al. (1998) for post-main-sequence evolution – have suggested an alternative explanation to dynamo saturation in that magnetic fields concentrated in polar starspots could be the reason for the lack of angular momentum loss. Solanki et al. (1997) presented numerical simulations that show that the effect of polar magnetic fields in the evolution of stellar rotation would be quantitatively the same as with a dynamo saturation process. The only way to find conclusive observational evidence for or against the polar field hypothesis is to Doppler image rapidly-rotating cluster stars and search for polar starspots. Cluster stars are especially important because, when intercompared in a narrow mass range, they should have had an identical history. Nevertheless, Pleiades UFRs of a single mass can show a range in surface rotation of a factor of 20 or more (Soderblom et al. 1993b). Recent

Send offprint requests to: K. G. Strassmeier,
e-mail: kstrassmeier@aip.de

⋆ Visiting Astronomer, Canada-France-Hawaii Telescope, operated by the National Research Council of Canada, the Centre National de la Recherche Scientifique de France, and the University of Hawaii.

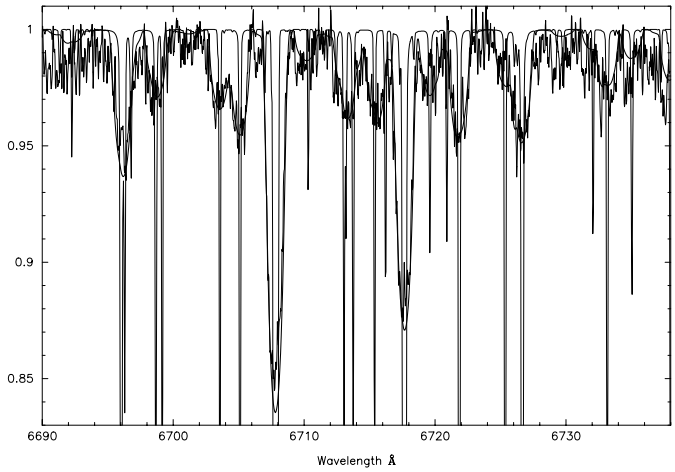

Fig. 1. Spectrum synthesis of the line region around Li I 6707.8 Å and Ca I 6717 Å. The spectral resolution is 65 000. The thin line is the unbroadened synthetic spectrum from a 5750 K/$\log g = 4.5$ model atmosphere computed with our altered transition probabilities. It demonstrates the amount of blending in this wavelength region. A trial-and-error fit with $v \sin i = 38$ km s^{-1}, $\xi = 2.0$ km s^{-1} and $\zeta = 1.5$ km s^{-1} is shown as a thick line.

correlative analysis suggests a rotation-induced lithium depletion for the Pleiades stars but not for younger clusters like α Per (Tschäpe & Rüdiger 2001), which is another intriguing question awaiting answer.

The primary aim of this paper is to search for a polar spot on one of the brightest, *solar-type*, rapid rotators in the Pleiades cluster and to relate the Doppler image to current flux-tube models.

2. Observations

High-resolution spectroscopic observations were obtained with the *Gecko* Coudé spectrograph at the 3.6-m Canada-France-Hawaii telescope (CFHT) in November 22–26, 1998. The 2048^2 Loral-5 CCD with 15 μm pixels and the dispersion of 1.6 Å/mm^{-1} provided a useful wavelength range of around 50 Å centered at 6713 Å. The spectrograph resolution was ≈120 000 but rebinning in the dispersion direction resulted in an effective resolution of 65 000 (4.6 km s^{-1}). Seeing was always between 0.6–1.2″ and all integrations were set at an exposure time of 3×17 min and have typical signal-to-noise ratios of 100–120:1. This sequence allowed for a total of 31 spectra well distributed over all rotational phases. Ultimately four of these spectra were eliminated from the analysis because they suffered from excessively low S/N. Figure 1 displays a typical spectrum. No water-vapor lines above the nominal noise level are obvious in these spectra and no attempts were made to correct for it. The reduction procedure was identical to that in our paper on LQ Hydrae (Rice & Strassmeier 1998) obtained with the same telescope and instrumental set up and we refer the reader to that paper.

The high spectroscopic resolving power results in 30 resolution elements across the full width of a photospheric absorption line which translates into a spatial resolution at the stellar meridian along the equator of approximately 2°. However, the exposure time of 51 min will cause phase smearing of up to a maximum of $0\overset{\text{p}}{.}023$ or 8° along the stellar equator and in the direction of the rotational motion.

3. Astrophysical data for HII 314

The photometric variability of HII 314 was discovered by Panov & Geyer (1991) but no period was obtainable from their data. During an extensive photometric monitoring program of the Pleiades cluster, Prosser et al. (1993) then detected a clear periodicity of 35.5 hours (1.48 days) with an amplitude of $0\overset{\text{m}}{.}1$ in 1992. The continuation of this program in 1993/94 led to a better sampled light curve and to a period of 1.47 days (Prosser et al. 1995). We use this period and an arbitrary zeropoint to phase our spectra

$$\text{HJD} = 2451141.0 + 1.47 \times E. \quad (1)$$

If the photometric period is interpreted as the stellar rotation period it yields – together with an independently measured $v \sin i = 41.9 \pm 1.6$ km s^{-1} from Queloz et al. (1998) – a value for the minimum radius of $R \sin i = 1.22 \pm 0.05\ R_\odot$ that seems to be inconsistent with the G1V classification and rather suggests a F7 spectral type. Even a value of 38 km s^{-1} (Soderblom et al. 1993b) does not solve the inconsistency and gives $R \sin i = 1.10\ R_\odot$. As noted by Ayres (1999) this disparity is even worse if the new Hipparcos distance for the Pleiades cluster of 118.3 ± 3.5 pc (Leeuwen 1999) is correct because then the luminosity of HII 314 would be only 0.72 $L_\odot$ (with B.C. $= -0.069$; Flower 1996 and $A_V = 3.2\,E(B-V) = 0\overset{\text{m}}{.}13$). The absolute magnitude would be $+5\overset{\text{m}}{.}0$ (from $V = 10\overset{\text{m}}{.}56$) which suggests a G4-5 star with a radius of 0.965 $R_\odot$ instead of a G1-2 classification. However, the dereddened color of $(B-V)_0 = 0\overset{\text{m}}{.}613$ (Soderblom et al. 1993a) strongly suggests a G1-2V classification. According to the color-temperature calibration of Flower (1996), a $B-V$ of $0\overset{\text{m}}{.}613$ corresponds to an effective temperature of 5845 K. Even if we adopt the "main-sequence-fitting" (MSF) distance of 132 pc (Pinsonneault et al. 1998; Terndrup et al. 2000) the luminosity is 0.895 $L_\odot$, according to a G3 dwarf, but its radius of 0.99 $R_\odot$ is still in disagreement with $R \sin i = 1.10\ R_\odot$. The latter may not be a too strong an inconsistency because the definition of radii of rapidly-rotating pre-main-sequence stars with left-over disc material could be different than for normal main-sequence stars.

Note that the star is not a binary even though Soderblom et al. (1993b) presented two radial-velocity measurements that differed by 3.5 km s^{-1} with respect to each other and therefore listed HII 314 as a possible single-lined spectroscopic binary. Table 1 lists our new CFHT radial velocities and we find the star to be constant in radial velocity, and thus most likely single. The new average velocity of $+4.4 \pm 0.6$ (rms) km s^{-1} is within the range of

Table 1. Spectroscopic observing log and radial velocities.

HJD	Phase (Eq. (1))	Phase in degr. (Fig. 3)	v_r ($km\,s^{-1}$)	error
2451140.98127	0.668	240	+3.1	2.3
2451141.76696	0.203	73	+3.7	4.4
2451141.80450	0.229	82	+3.8	3.8
2451141.84247	0.254	91	+3.4	2.8
2451141.88715	0.284	102	+3.7	4.3
2451141.92464	0.310	111	+4.3	2.9
2451141.96193	0.335	120	+4.1	2.1
2451141.99959	0.360	129	+4.2	2.6
2451142.03727	0.387	139	+4.2	3.4
2451142.07509	0.413	148	+4.3	3.8
2451142.11255	0.439	...	+4.6	3.2
2451142.75714	0.876	315	+3.9	4.4
2451142.79633	0.903	325	+4.5	3.9
2451142.83377	0.928	334	+4.8	2.8
2451142.87275	0.955	343	+4.9	3.0
2451142.91437	0.984	354	+4.6	2.8
2451142.96315	0.016	5	+5.0	2.4
2451143.00326	0.044	15	+5.0	2.9
2451143.04044	0.069	24	+5.3	3.0
2451143.07773	0.094	33	+4.7	3.2
2451143.11541	0.120	...	+4.4	3.7
2451143.74473	0.548	197	+3.6	3.1
2451143.78196	0.573	206	+3.9	2.6
2451143.81952	0.595	214	+3.6	3.1
2451143.85679	0.624	224	+4.9	3.0
2451143.89470	0.650	234	+5.0	3.4
2451143.93200	0.676	243	+5.1	3.3
2451143.96934	0.701	252	+5.3	4.2
2451144.01719	0.733	263	+4.8	2.9
2451144.06050	0.763	274	+5.2	3.9
2451144.09771	0.788	...	+4.7	2.8
Average			+4.4	

the two velocities from Soderblom et al. (1993b). It confirms cluster membership of HII 314 despite the offset of $-1.6\,km\,s^{-1}$ from the mean cluster velocity of $+6.0\,km\,s^{-1}$ (Narayanan & Gould 1999; Terndrup et al. 2000).

The average equivalent width of the lithium line at 6708 Å is 173 ± 8 (rms) mÅ and that of the Ca I 6717-Å line is 163 ± 12 mÅ. The latter is more difficult to measure because of the larger number of blends (see Fig. 1). For the lithium line, the critical blend at 6707.441 Å is – we believe – synthesized properly and is made up of mostly a V I and a Fe I contribution. Soderblom et al. (1993a) measured an equivalent width for the lithium line of 167 ± 18 mÅ (and obtained $\log n(\mathrm{Li}) = 3.15$) and for the calcium line of 157 ± 18 mÅ, in good agreement with our measures. The value of 173 ± 8 mÅ converts with the non-LTE tables of Pavlenko & Magazzù (1996) into a logarithmic abundance of 3.13 ± 0.09.

The Hα profile of HII 314 appears as a weak and asymmetric absorption profile with a total equivalent width of ≈1.1 Å. The two spectra obtained by Soderblom et al. (1993a) showed significant line-core variations which indicate that the star has an active chromosphere with plages and flares. A remarkable flare was detected in the C IV line with HST (Ayres et al. 1994) and its coronal X-ray emission is known since *Einstein* (Micela et al. 1990) and the ROSAT all-sky survey (Hünsch et al. 1999) giving $\log L_X = 30.3\,erg\,s^{-1}$. Preibisch (1997) obtained a coronal temperature of $\log T = 7.8$ K which is 25 times higher than the "typical" solar value. The star is also a radio continuum emission source and appears in the catalog of Wendker (1995).

4. A Doppler image for November 1998

4.1. The TempMap code

Our Doppler imaging program (TempMap) is based on the code by Rice et al. (1989) (also described in Piskunov & Rice 1993). Extensive numerical tests and an update of the program's primary capabilities were recently presented by Rice & Strassmeier (2000). For details, we refer the reader to this and previous papers in this series.

For the present paper, TempMap was extended to work in a larger wavelength range than the previous applications with mostly a single main spectral line of roughly ±1 Å per inversion. A total of up to 24 Å of spectrum with some forty lines including the Li I 6707 and Ca I 6717 lines were used in the input. The inclusion of large portions of continuum with basically no stellar surface information requires the additional input of a weight for each of the 701 pixels in the spectrum. We averaged flux over 15 pixels around each single pixel and if the average of the normalized residual intensity, I_{average}, was less than 0.01 the weight was 0.1, if between 0.01–0.05 the weight was based on the formula $(I_{\mathrm{average}} - 0.01) * 22.5 + 0.1$, and if over 0.05 the weight was 1.0. This ensures that the continuum regions receive less weight and the spectral lines comparably higher weight the closer a pixel appears to the line core. Note that we did not apply this weighting scheme for the single-line inversions because, firstly, it is intended to save CPU time by excluding large portions of continuum which does not apply to the single-line inversions and, secondly, we wanted to compare the large-wavelength inversion with our previously published single-line images that did not include a weighting scheme. We had run a few test inversions with and without weighting and found no systematic differences.

4.2. Input parameters

The radiative transfer in our program is based on ten model atmospheres with temperatures from 3500 K to 6500 K taken from the ATLAS-9 grid (Kurucz 1993). A gravity of $\log g = 4.5$ and a microturbulence of $2.25\,km\,s^{-1}$ were adopted based on the G2V spectral classification of HII 314 and its young age. Further stellar parameters are listed in Table 2.

The final solution considers a total of 38 lines in the inversion simultaneously. The atomic data for these lines

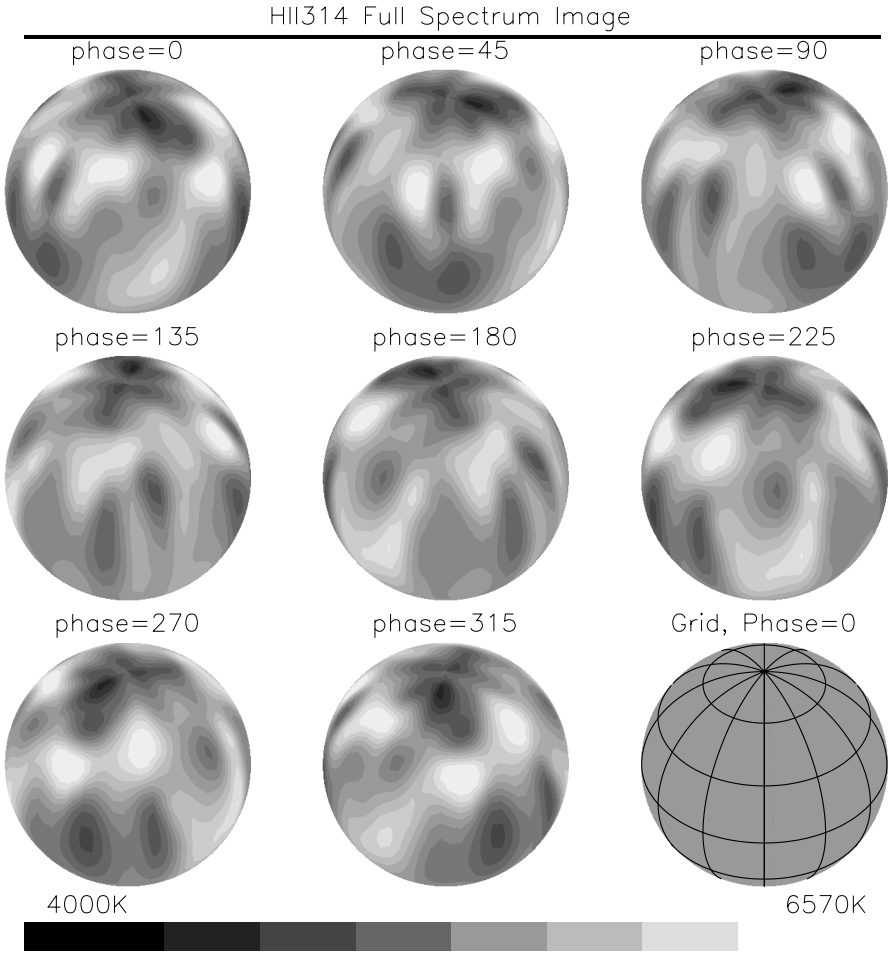

Fig. 2. Doppler image of HII 314 from a 20-Å piece of spectrum including the Li I 6707 Å and the Ca I 6717 Å lines. Maps are plotted in a spherical projection at eight equidistant rotational phases. The temperature scale is indicated and is the same for all projections.

Table 2. Astrophysical data for HII 314.

Parameter	Value
Spectral type	G1–2V
Distance (Hipparcos)	118.3 ± 3.5 pc
Distance (MSF)	132 pc
M_V	$+5\overset{\mathrm{m}}{.}19 \pm 0.06$ (Hipparcos)
$\log g$	4.5 ± 0.2
$(B-V)_0$	$0\overset{\mathrm{m}}{.}613$
$T_{\rm eff}$	5845 K (from $B-V$)
$v \sin i$	38.7 ± 1 km s^{-1}
Rotation period	1.47 days
Minimum radius $R \sin i$	1.12 ± 0.04 $R_\odot$
Inclination	50° (adopted)
Macroturbulence, ζ	4.5 km s^{-1}
Microturbulence, ξ	2.25 km s^{-1}

were taken from VALD (Vienna Atomic Line Database; Kupka et al. 1999). Abundances for the many chemical elements within the useable spectral range were kept at the solar value by default but the Ca and Li abundance were adjusted during the imaging. The values used in the final inversion are 3.0 for lithium and 6.32 for calcium (on the regular $\log n(\mathrm{H}) = 12.00$ scale). The latter is identical to the solar value within the estimated uncertainty of ≈0.07 dex.

The inclination of the rotational axis was estimated by running a series of inversions each optimized for a particular choice of inclination and then identifying the minimum in χ^2 (as was done in most previous papers in this series). For HII 314, the Ca line line produced a much broader χ^2 minimum than the Li line and we chose the final value (50°, Table 2) on the basis of best mutual agreement.

4.3. Results

Figure 2 shows our final map for HII 314 in a spherical projection style at eight equidistant phases. It includes the spectral information from both main mapping lines plus a total of 36 weaker lines (partially blended as shown in Fig. 1). No photometry was available for the inversion but a total of 27 spectra with S/N above 100:1 well distributed over all rotational phases within two consecutive stellar

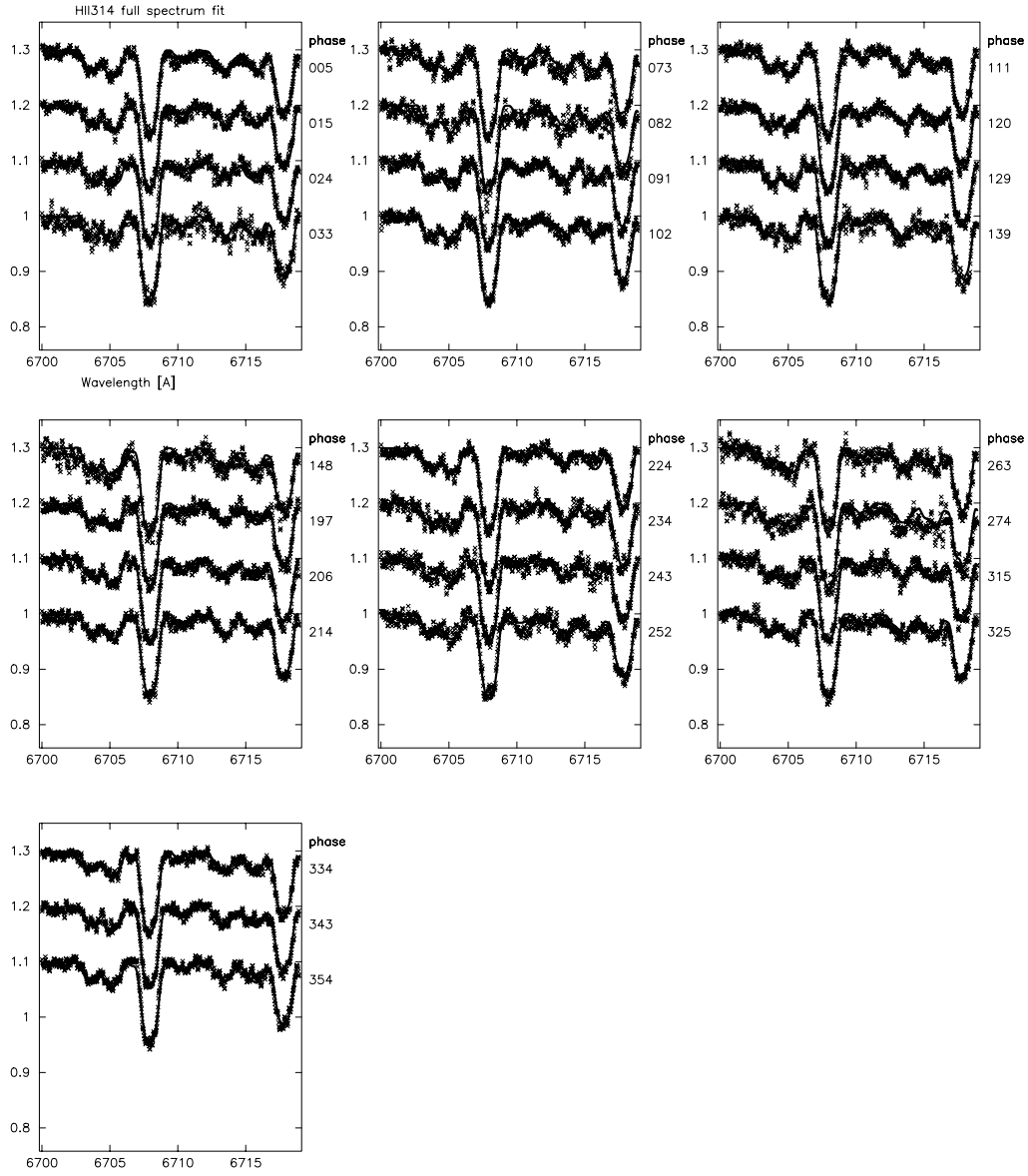

Fig. 3. Observed and computed line profiles from the full-spectrum inversion. The spectra are arranged with increasing phase and are labeled with surface longitude in degrees.

rotations (no phase gap is larger than $0\overset{p}{.}1$) are a tight constraint for the profile inversion. The fit to the data is shown in Fig. 3 for a 20-Å piece of spectrum. Its combined sum of the squared residuals was 1.93 for the final solution from 701 spectral data points. For comparison, Fig. 4 shows the single-line images from lithium and calcium. Its residuals were 0.202 from 81 spectral data points for Ca I 6717 Å and 0.184 for Li I 6707 Å, also for 81 spectral data points (the definition of TempMap's residuals is the same as in Kövari et al. 2001). The residuals normalized by the total number of spectral data points is thus comparable for the three maps.

Finding a satisfactory solution from each of the two main lines, that also compare well with that from the full spectrum, turned out to be a real challenge. The cause is not so much the inversion code (itself) and its free parameters, but rather the joint effects of a low S/N ratio and unknown and uncorrectable external uncertainties in the data (see Rice & Strassmeier 2000). We thus consider our final map of HII 314 more uncertain than previous maps in this series but still emphasize that this is the best that the data would allow. Further progress could be made with the least-squares deconvolution process put forward by Donati et al. (1997) but at the costs of losing the temperature information.

The map in Fig. 2 shows individual features mostly at high and low latitudes, including an elongated polar finger crossing from one side of the pole to the other near a longitude of $\ell \approx 315°$. The average spot temperature appears to be near 4700 K, with a few areas as cool as 4400 K and some with upper limits of approximately 5400 K. Several warm/bright regions seem to be present but are suspicious due to the relatively low S/N ratio of our spectra. Also, these features mostly appear as counterparts to cool

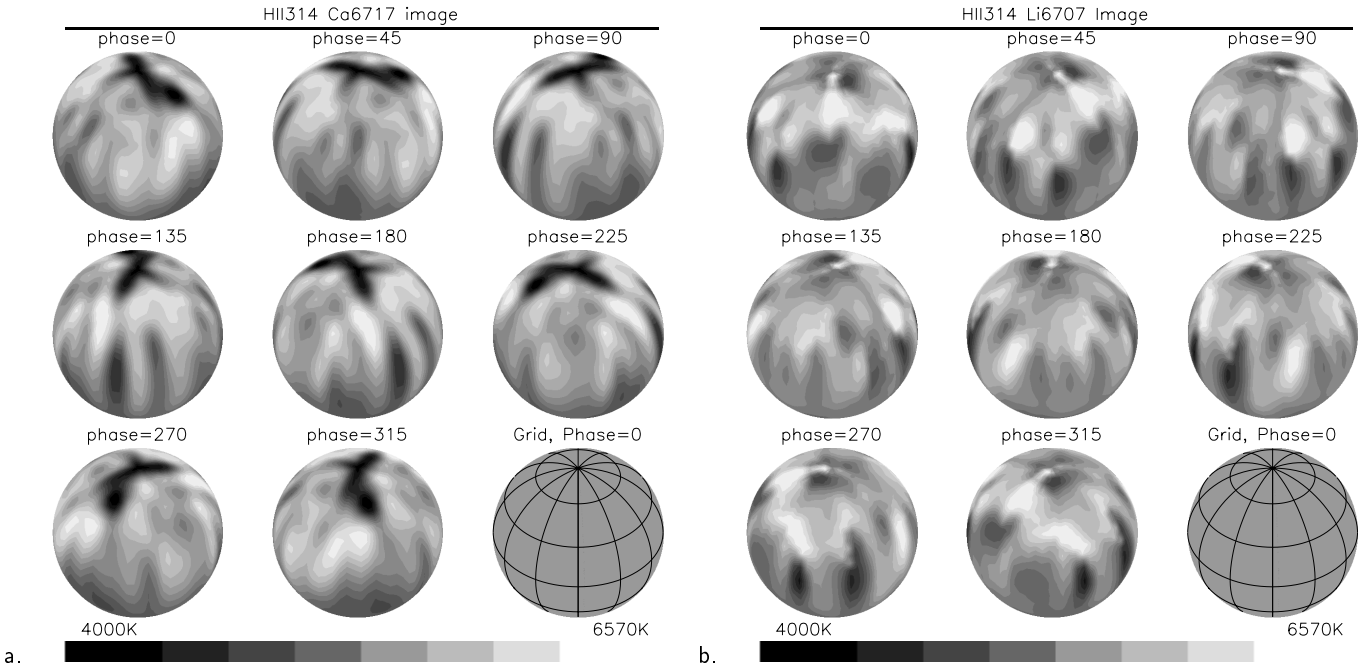

Fig. 4. Single-line Doppler images from **a)** the Ca I 6717 Å line and **b)** the Li I 6707 Å line.

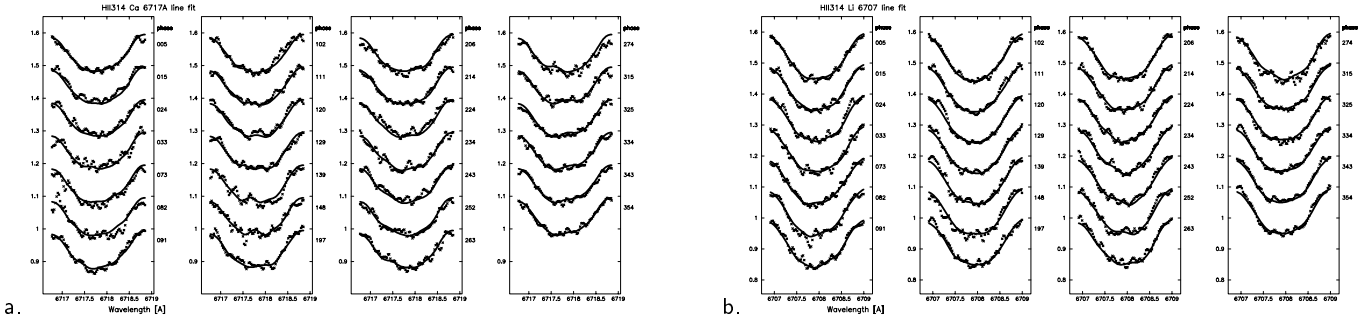

Fig. 5. Observations and fits from the single-line inversions. **a)** the Ca I 6717 Å line, **b)** the Li I 6707 Å line.

spots along meridional circles. This is typical behavior for a maximum-entropy regularized solution, which requires that the total image entropy is maximized while the residuals between fit and data are minimized. This is most easily done by the code by putting hot spots adjacent to dominant cool spots. Despite this, we tried various input parameter combinations to fully remove or enhance such features without significantly deteriorating the quality of the fit at the same time (these were mostly variations in elemental abundance, $v \sin i$, and blend characteristics like transition probabilities). Their surface location, however, varied significantly from one reconstruction to another and we are not confident of their reality even though the single-line inversions also recover them but with differing contrast. Also, there is a good possibility that these features are, at least partly, due to the well-known north-south mirroring effect in Doppler imaging (see, e.g., Vogt et al. 1987). In the end, we conclude that these bright features are artifacts due to the low S/N of our spectra.

A comparison of our two single-line images is made in Fig. 4. The fits are shown in Fig. 5 to allow for a phase-to-phase comparison with the full-spectrum fit. This helps the reader to judge the significance of the maps. However, we emphasize that the Li I-6707 line is special, firstly because of its zero lower excitation potential and secondly, it consists of a close doublet of two isotopes not resolved at the large rotational broadening of HII 314.

Figures 6 and 7 represent a consistency check for the two single-line maps. This check is made by inverting even numbered profiles and odd numbered profiles separately and then comparing the respective output maps. While the Ca I-6717 line produces consistent "even" and "odd" maps, the Li I-6707 line did not. The reason is an accidental untimely alignment of several noise spikes and any residual effects of removed cosmic-ray hits in the even-numbered Li profiles that are interpreted by the code as real surface features corotating with the star (mostly around phases of ≈270°). This can only happen if the S/N ratio is low, otherwise the code realizes the inconsistency during the fitting of adjacent, nonaffected, phases. Even though the solution from the full number of profiles weakens these artifacts, the full-spectrum map in Fig. 2 still shows two spots where the Ca maps and the odd-numbered Li map shows none. At this point, we decided

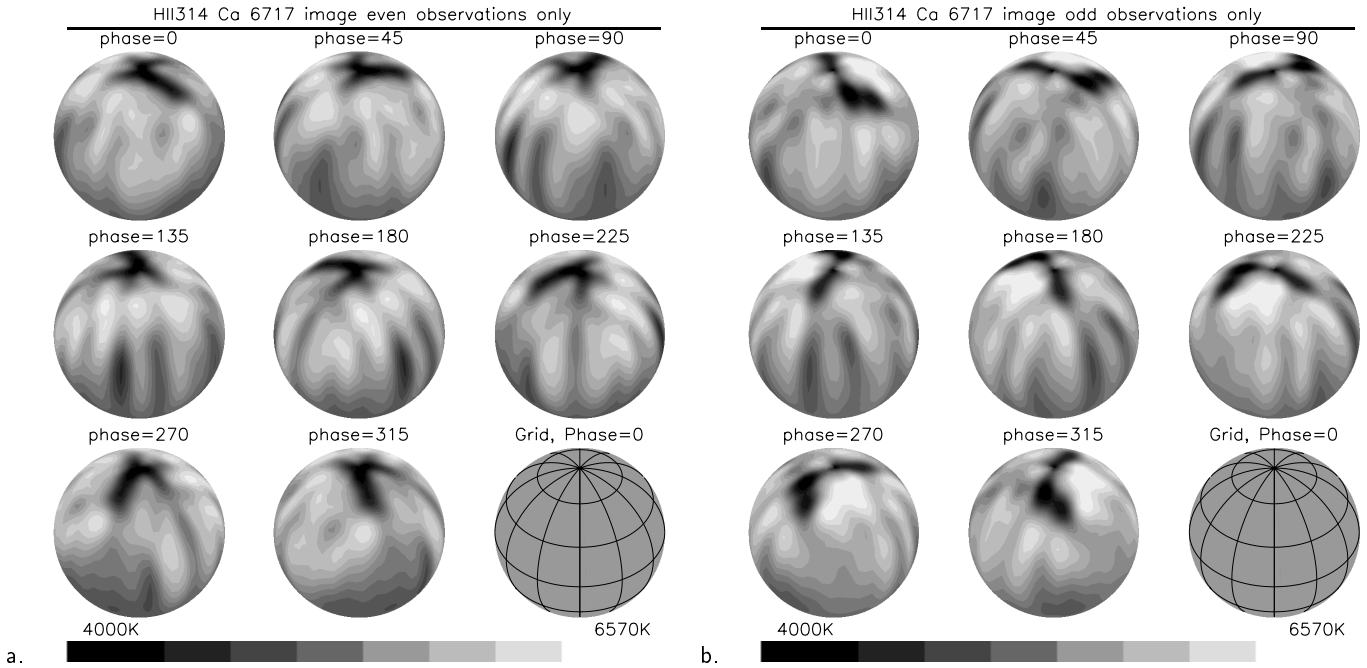

Fig. 6. Single-line Doppler images from the Ca I 6717 Å line for **a)** the even numbered phases and **b)** the odd numbered phases.

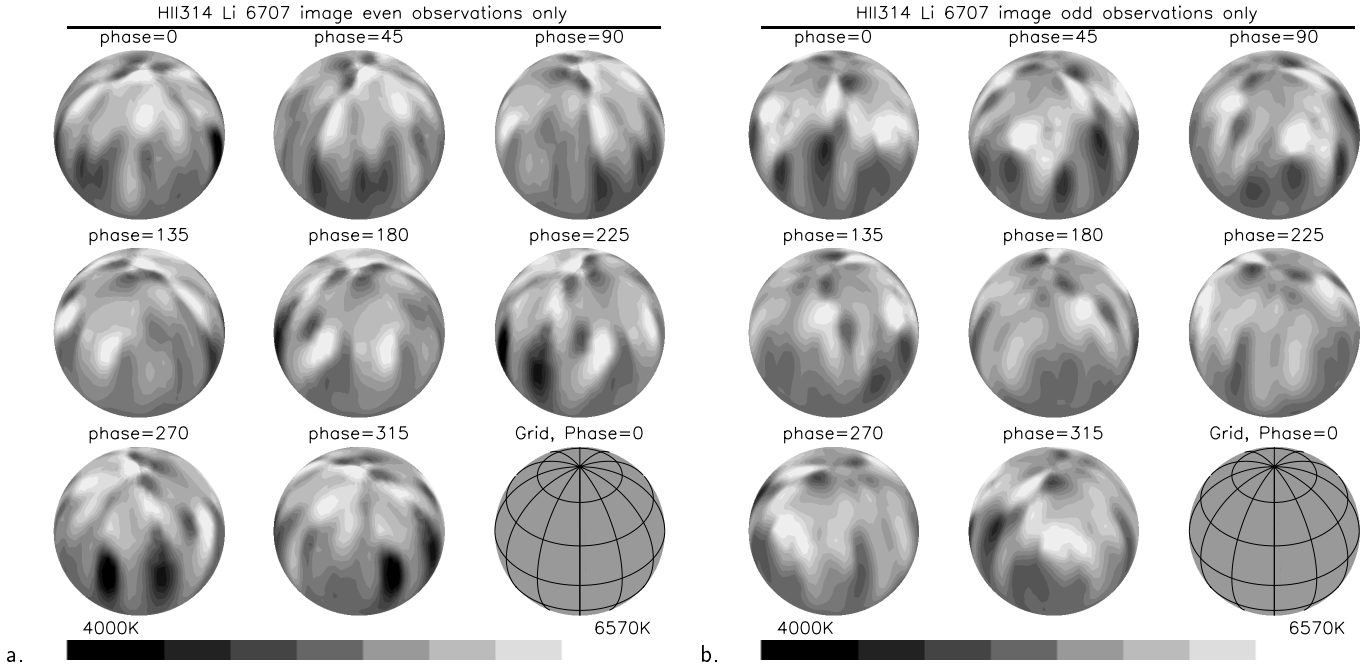

Fig. 7. Single-line Doppler images from the Li I 6707 Å line for **a)** the even numbered phases and **b)** the odd numbered phases.

to show the result as is (without trying to fiddle around with cleaned data etc.) but caution the reader that the two spots at around a longitude of $\ell \approx 270°$ are artifacts from the even-numbered Li profiles.

Finally, we compared the average of the two single-line maps with the full-spectrum image. It shows that the standard-deviation for each surface grid element is always below 100 K. This value would be the external uncertainty expected for inversions with spectra of the order of $S/N \approx 100$:1, as demonstrated in the forward and inverse simulations by Rice & Strassmeier (2000). We are thus confident not to have overregularized the final map. Both standard-deviation maps appear with the largest inconsistencies at or near the pole and at $\ell \approx 270°$ where the even-numbered Li profiles recover two equatorial features, as discussed above. Although these sigma maps are by no means formal "error maps", they still allow an estimate of the external errors per surface resolution element and are a useful tool to judge the reliability of particular surface features.

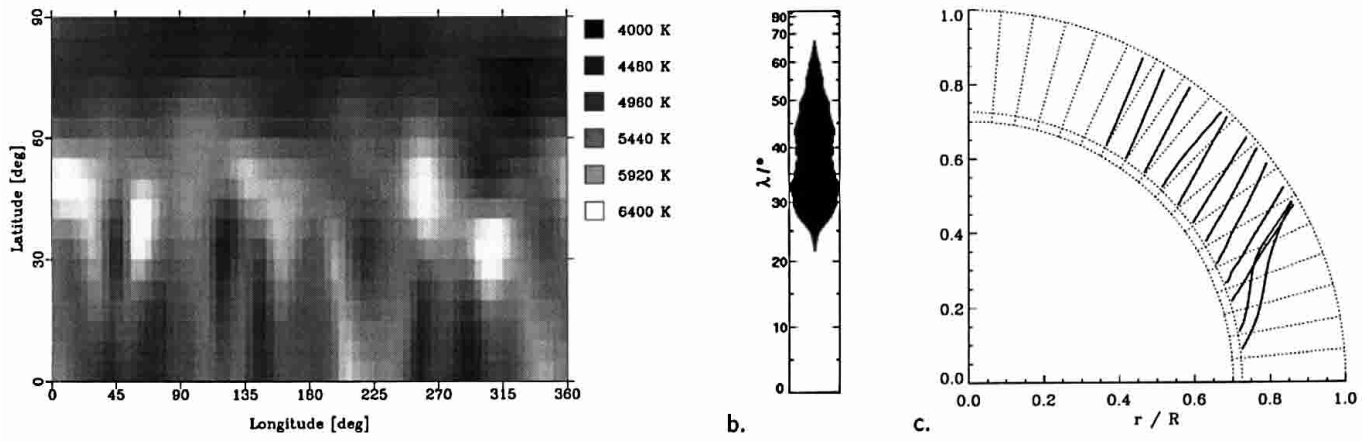

Fig. 8. A comparison of our Doppler image **a)** with theoretical predictions **b)** and **c)**. The computed latitude distribution of emerging flux tubes for a one solar-mass star with the rotation rate of HII 314 ($\Omega = 18\,\Omega_\odot$) is shown in panel **c)** as a radial cross section with the trajectories of the summit of rising flux loops. Panel **b)** shows the spot probability as a function of latitude (a larger width means a higher surfacing probability).

5. Discussion

Solar-type open-cluster stars are typically as faint as $V = 13$ mag and even fainter, and present an observational challenge for high-resolution high-S/N spectroscopy because successful Doppler imaging requires relatively short observational integration times in order to minimize phase smearing during the exposure. Consequently, only a few attempts have been made to map such stars despite the importance they have because of their well-established stellar age. Stout-Batalha & Vogt (1999) presented Doppler images of the low-mass Pleiads HII 686 (K6V) and HII 3163 (K0V) from 10-m Keck data while Barnes et al. (1998) mapped the two G-type α-Per stars He699 and He520 with the help of their least-squares deconvolution technique. Large polar spots were found on all four of these stars. A multi-line analysis of the less rapidly rotating G1.5V field star EK Dra (Strassmeier & Rice 1998) also yielded a polar spot, although weaker and in addition to very high-latitude spot features. Unfortunately, we can still not compare all these images quantitatively because: 1) There is a large range of rotation periods covered (from 0.397 days for HII 686 to 2.6 days for EK Dra). 2) Their effective temperatures and masses differ by a factor of two (one solar mass for the early G stars down to ≈0.6 solar masses for HII 686). 3) There is a significant age difference between the 100–120 Myr of the Pleiades cluster, the 50–70 Myr of the α Per cluster, and the basically unknown but likely greater age of a field-G star of similar mass. Despite these astrophysical diversities, are there any observational similarities of the surface spot distributions?

It appears not! Our new image of a moderately rapidly-rotating and, for this group, intermediate-age G star at least allows a direct comparison with our previous image of EK Dra and the α-Per G stars in Barnes et al. (1998). One feature that is common to all these stars is their polar spot or, if one wishes, their very high latitude spot appearance. Not surprisingly due to the large stellar diversity, neither of the spot distributions on these stars are in full agreement with the flux-tube models put forward by Schüssler et al. (1996) for main-sequence (MS) stars, and later by Granzer et al. (2000) for pre-main-sequence stars. The discrepancy observed is mostly due to the coexistence of equatorial spots and polar spots at the same time, while the MS and ZAMS models with $\Omega >> \Omega_{\rm Sun}$ usually predict spots at intermediate and moderately high latitudes but none on the equator or at the poles. Of course, the models are still based on the assumption that all flux tubes start in an overshoot layer at latitudes below 60° because only then does the model reproduce the solar spot distribution. In this framework, truly polar spots can only appear in very cool and rapidly-rotating pre-main-sequence stars with ultra-deep convection zones (down to 0.1 of the stellar radius; Granzer et al. 2000). However, Belvedere et al. (1998) had suggested that, if the overshoot layer is sufficiently thick, a boundary-layer dynamo would be located at all latitudes, i.e. also above 60°, and thus magnetic flux would be likely to surface directly at the poles as well. Recent helioseismic studies of the solar tachocline suggest temporal and latitudinal variations of its width in the sense that it is located deeper at the equator than at the poles (e.g. Corbard 2001), thus lending some support to the 60° assumption, at least for the Sun.

Figure 8 is an attempt to compare the observed Doppler image of HII 314 with a flux-tube simulation for the specific stellar parameters and rotational velocity of HII 314. Because of the still remaining inconsistency between the luminosity from the Hipparcos parallax and that from ground-based spectroscopic data, we adopt the model of a one solar-mass star and emphasize that a range of $\pm 0.2\ M_\odot$ does not significantly affect the flux-tube paths (see Granzer et al. 2000). Thus, the only difference to the solar case is the 18-times higher angular velocity of HII 314. The convection zone is assumed to behave as a rigid rotator and the initial field strength at

the bottom of the convection zone is chosen so that the magnetic flux reaches values typical for large solar active regions (10^{14} Wb). As one can see from Fig. 8, the model does not predict magnetic surface flux above a latitude of 60°–65°, in obvious disagreement with the observation, and also does not predict flux below a latitude of ≈25°, also in disagreement with our observations. The question whether the "warm" equatorial features in our image are real – warm with respect to the effective temperature as discussed in Sect. 4.3 – or are just spotless i.e. magnetic-field free regions still remains to be determined. At the moment, we conclude that these features are artifacts due to the comparably low S/N of our spectra.

It is the stellar equator and the polar regions that are also the most uncertain regions in our Doppler images showing rms deviations of up to 100 K as compared to below 40 K on average for the other regions. Also, the current flux-tube models terminate ≈2% of the stellar radius below the observable surface because the thin flux-tube approximation breaks down and thus a direct comparison with surface observations always remains incomplete. Furthermore, no information of field geometry – radial versus azimuthal – enters into the comparison with our Doppler image. It is thus not surprising that we do not find perfect agreement between theory and observation but emphasize that further progress could not only come from better observational data but also from the inclusion of the surface-field geometry in flux-tube emergence models. The latter being linked to the implementation of a thick flux-tube replacement for the flux transportation in the outermost layers and with the existence and treatment of global shear flows like meridional circulation at or near the stellar surface (see e.g. Miesch et al. 2000; Küker et al. 2001). The location of the stellar dynamo itself is yet another uncertainty.

Acknowledgements. K. G. Strassmeier is very grateful to the German Science Foundation (DFG) for support under grant STR645/1-1 and the Austrian Science Foundation (FWF) for support under grants S7301-AST and S7302-AST. J. B. Rice acknowledges support from the Natural Science and Engineering Research Council of Canada (NSERC). We thank Th. Granzer for computing the MHD models.

References

Ayres, T. R. 1999, ApJ, 525, 240
Ayres, T. R., Stauffer, J. R., & Simon, T. 1994, ApJ, 420, L33
Barnes, J. R., Collier Cameron, A., Unruh, Y. C., Donati, J.-F., & Hussain, G. A. J. 1998, MNRAS, 299, 904
Barnes, S., & Sofia S. 1996, ApJ, 462, 746
Belvedere, G., Lanza, A. F., & Sokoloff, D. 1998, SP, 183, 435
Buzasi, D. L. 1997, ApJ, 484, 855
Corbard, T. 2001, ESA SP-463, in press
Donati, J.-F., Semel, M., Carter, B. D., Rees, D. E., & Collier Cameron, A. 1997, MNRAS, 291, 658
Flower, P. J. 1996, ApJ, 469, 355
Granzer, Th., Schüssler, M., Caligari, P., & Strassmeier, K. G. 2000, A&A, 355, 1087
Hünsch, M., Schmitt, J. H. M. M., Sterzik, M. F., & Voges, W. 1999, A&AS, 135, 319
Keppens, R., MacGregor, K. B., & Charbonneau, P. 1995, A&A, 294, 469
Kövari, Z., Strassmeier, K. G., Weber, M., Washuettl, A., & Rice, J. B. 2001, A&A, 373, 199, Paper XV
Küker, M., Rüdiger, G., & Schultz, M. 2001, A&A, in press
Kupka, F., Piskunov, N. E., Ryabchikova, T. A., Stempels, H. C., & Weiss, W. W. 1999, A&AS, 138, 119
Kurucz, R. L. 1993, ATLAS-9, CD-ROM #13
Mestel, L. 1999, Stellar Magnetism, Oxford Science Publ. (Clarendon Press), Oxford
Micela, G., Sciortino, S., Vaiana, G. S., et al. 1990, ApJ, 348, 557
Miesch, M. S., Elliott, J. R., Toomre, J., et al. 2000, ApJ, 532, 593
Narayanan, V. K., & Gould, A. 1999, ApJ, 515, 256
O'Dell, M. A., Panagi, P., Hendry, M. A., & Collier Cameron, A. 1995, A&A, 294, 715
Panov, K. P., & Geyer, E. H. 1991, A&A, 242, 112
Pavlenko, Y. V., & Magazzù, A. 1996, A&A, 311, 961
Pinsonneault, M., Stauffer, J., Soderblom, D. R., King, J. R., & Hanson, R. B. 1998, ApJ, 504, 170
Piskunov, N. E., & Rice, J. B. 1993, PASP, 105, 1415
Preibisch, T. 1997, A&A, 320, 525
Prosser, C. F., Shetrone, M. D., Marilli, E., et al. 1993, PASP, 105, 1407
Prosser, C. F., Shetrone, M. D., Dasgupta, A., et al. 1995, PASP, 107, 211
Queloz, D., Allain, S., Mermilliod, J.-C., Bouvier, J., & Mayor, M. 1998, A&A, 335, 183
Rice, J. B., & Strassmeier, K. G. 1998, A&A, 336, 972, Paper VII
Rice, J. B., & Strassmeier, K. G. 2000, A&AS, 147, 151
Rice, J. B., Wehlau, W. H., & Khokhlova, V. L. 1989, A&A, 208, 179
Schüssler, M., Caligari, P., Ferriz-Mas, A., Solanki, S. K., & Stix, M. 1996, A&A, 314, 503
Soderblom, D. R., Jones, B. F., & Balachandran, S. 1993a, AJ, 106, 1059
Soderblom, D. R., Stauffer, J. R., Hudon, J. D., & Jones, B. F. 1993b, ApJS, 85, 315
Solanki, S. K., Motamen, S., & Keppens, R. 1997, A&A, 324, 943
Stauffer, J. R., Hartmann, L. W., Soderblom, D. R., & Burnham, J. N. 1984, ApJ, 280, 202
Stout-Batalha, N. M., & Vogt, S. S. 1999, ApJS, 123, 251
Strassmeier, K. G., Bartus, J., Kővári, Z., Weber, M., & Washuettl, A. 1998, A&A, 336, 587, Paper VIII
Strassmeier, K. G., & Rice, J. B. 1998, A&A, 330, 685, Paper VI
Terndrup, D. M., Stauffer, J. R., Pinnsonneault, M. H., et al. 2000, AJ, 119, 1303
Tschäpe, R., & Rüdiger, G. 2001, A&A, in press
van Leeuwen, F. 1999, A&A, 341, L71
Vilhu, O. 1984, A&A, 133, 117
Vogt, S. S., Penrod, G. D., & Hatzes, A. P. 1987, ApJ, 321, 496
Wendker, H. J. 1995, A&AS, 109, 177